Affordable and sustainable new generation of solar cells: calcium titanate ($CaTiO_3$) – based perovskite solar cells

Alfonsina Abat Amelenan Torimtubun[1], *Anniza Cornelia* Augusty[1], *Eka* Maulana[2], and *Lusi* Ernawati[1,*]

[1]Department of Chemical Engineering, Institut Teknologi Kalimantan, Balikpapan 76127, Indonesia
[2]Department of Electrical Engineering, University of Brawijaya, Malang 65145, Indonesia

Abstract. Indonesia is located along the equator lines with the high intensity of solar radiation averaging about 4.5 kWh of electrical energy/day. This potential leads to the self-sustaining energy possibility fulfilling the electricity needs. Due to their unique electronic structures and high-cost merit over the existing commercial PV technologies, perovskite solar cells (PSCs) have emerged as the next-generation photovoltaic candidate. Their highest power efficiency can be achieved of up to 22.1% in the last 5-6 years. However, this high efficiency came from $CH_3NH_3PbI_3$ materials which contain lead, a toxic material. Herein calcium titanate (CT) as a lead-free perovskite material were synthesized through sintering of calcium carbonate ($CaCO_3$) and titanium oxide (TiO_2) by the sol-gel method. CT powders were characterized by SEM, XRF, FTIR and XRD then applied it onto the mesoporous heterojunction PSCs, with a device architecture ITO/TiO_2/$CaTiO_3$/C/ITO. By manipulating the raw material stoichiometry and heating temperature in the synthesis of $CaTiO_3$, the device shows the highest power conversion efficiency (PCE) of 2.12%, short-circuit current density (J_{SC}) of 0.027 mA cm^{-2}, open circuit voltage (V_{OC}) of 0.212 V and fill factor (FF) of 53.90%. This sample can be an alternative way to create lead-free, large-scale, and low-cost perovskite solar cells.

1 Introduction

Indonesia is a tropical country located along the equator line which receives a lot of solar energy every year. Most of Indonesian areas get a quite intense of solar radiation with the average daily radiation about around 4 kWh/m^2 [1]. For Indonesia which has a lot of small and isolated islands where electricity demand is quite low, photovoltaic solar energy system is one of solutions to meet Indonesia electricity needs [2].

The current generation of photovoltaics is perovskite solar cells (PSCs) that developed very rapidly in the past few years due to the outstanding semiconductor photoelectric properties of organic-inorganic perovskite materials and exceptional efforts in perovskite material and device investigation [3]. In 2009, research conducted by Miyasaka et al. employed the lead perovskite, $CH_3NH_3PbI_3$ ($MAPbI_3$), as light absorbers in the solar cells and demonstrated a power efficiency (PCE) of 3.8% [4]. Then, in just 7 years, the maximum PCE of PSCs has rapidly improved from 3.8% to 22.1%, now rivalling the efficiency of silicon solar cells [5]. However, compared to its high efficiency, material stability issue and toxicity of lead have remarkably limited its further step toward commercialization [6].

Calcium titanate ($CaTiO_3$) is one of the perovskite materials with the general formula of ABX_3, the cation A is occupied in a cube-octahedral site and the cation of B is occupied in an octahedral site where X is halide [7]. $CaTiO_3$ also shows dielectric properties with a relative permittivity value of up to 186 and the band gap of 3.8 – 4.00 eV which can be used as a optoelectronic device [8]. Depend on the phase transition temperatures, $CaTiO_3$ can be divided in four space groups: orthorhombic (Pbnm), orthorhombic (Cmcm), tetragonal (I4/mcm) and cubic (Pm3 m) [9]. Among them, cubic phase formed in the high temperature ($T > 1300°C$), tetragonal phase is a transient compound which formed in very limited temperature ($1250°C < T < 1349°C$), while the orthorhombic phase (Pbnm) is stable at room temperature [9–11].

The raw material sources of titanium in the synthesis of calcium titanate are minerals rutile, ilmenite and anatase and its main features are: rutile is a scarce mineral, it crystallizes in the tetragonal system and a density of 4.18 to 4.25 g/cm^3. Ilmenite presented hexagonal crystallization and rhombohedra, and a density of 4.10 to 4.80 g/cm^3 [9]. While anatase showed tetragonal system and a density of 3.79 to 3.97 g/cm^3 [12]. Luttrell et al.[13] showed that anatase has a larger band gap than rutile TiO_2 due to the different surface orientation, thus it is generally accepted that anatase exhibits a higher photoactivity than those of rutile.

* Corresponding author: lusiernawati@itk.ac.id

$CaTiO_3$ perovskite structure can be obtained by several synthesis methods such solid state reaction method [14], co-precipitation method [15], wet-chemical method (sol-gel) [16] and hydrothermal technique [17]. Sol-gel method provides important benefits over the other techniques due to the low cost, easy preparation route, tuneable composition control, high crystal homogeneity and lower temperature of crystallization [18]. However, undesired phase due to unreacted precursors are the drawbacks beside the loss of stoichiometry and wide particle size problems [19]. Hence, some process modifications are needed to ensure their reproducibility for mass production.

This study was thoroughly investigated the structural and physicochemical properties of $CaTiO_3$ powders which were synthesized using sol-gel method. Later, the paste form of the synthesized $CaTiO_3$ are deposited in an active perovskite layer for the lead-free PSCs application. The effect of the heat treatment temperature and $CaCO_3$:TiO_2 stoichiometric ratio in the synthesis of lead-free $CaTiO_3$ perovskite material were examined in order to improve PSCs device performance.

2 Experimental Methods

2.1. Materials

$CaTiO_3$ powder were synthesized by reacting the commercial $CaCO_3$ powder and TiO_2 anatase powder obtained from MTI Corporation (99%) with the solvent of ethanol purchased from (96%) Merck Milipore Corporation. Potassium iodide (KI) (0.5 M) and iodine solution (I_2) (0.05 M) as an electrolyte solution was purchased from Nirwana Abadi Surabaya and Fadjar Kimia Bogor trading business, respectively. All the chemicals mentioned above, except for $CaTiO_3$, were directly used without further purification. Graphite was used as a source of carbon from candle soot as the counter electrode. Indium Tin Oxide (ITO) glass (ITO-P008-1, Zhuhai Kaivo Optoelectronic Technology Co. Ltd., Guangdong, China) were used as a substrate with the resistivity of 18 – 24 Ω sq^{-1}.

2.2 Synthesis of $CaTiO_3$ Powder

Each $CaCO_3$ powder and TiO_2 powder (1:7 molar fraction) were dissolved in ethanol and stirred for 2 h at room temperature. The slurries were then dried in a 100°C oven for 1 h. The mixed powders were crushed then sintered by furin air at 900°C for 2 h, with the ramp rate of 3°C/min to obtain fine powder of $CaTiO_3$.

2.3 Device Fabrication

PSCs devices based on $CaTiO_3$ were fabricated in the ITO/TiO_2/$CaTiO_3$/C/ITO mesoporous heterojunction configuration. An ITO glass were sequentially cleaned with a mild detergent, distilled water and ethanol in ultrasonic bath. In addition, the $CaTiO_3$ paste was prepared by dissolving $CaTiO_3$ into ethanol and stirred until completely dissolved at room temperature. The TiO_2 and $CaTiO_3$ paste were deposited onto the cleaned ITO substrate by dip-coating technique, sequentially. Then, carbon was coated as a counter electrode. KI and I_2 solution were dropped onto the surface of active area of the PSCs. The device active area was 11.1 cm^2.

2.4 Characterization

X-Ray Diffraction (XRD) patterns were obtained using a PANalytical type X'Pert Pro diffractometer with Cu-Kα as the radiation source. Samples were scanned between 10 and 100° in 2θ with a resolution of 0.05°, 40 kV, and 40 mA. Crystal size was measured by Scherrer equation. SEM image of $CaTiO_3$ powder were measured by scanning electron microscopy (SEM, FEI type Inspect 21). The measurement conditions were 100 kV at various magnifications, as shown on scale bar of the images. The elemental analysis was performed using NEX QC+QuantEZ type of Rigaku X-Ray Fluorescence (XRF) and Fourier-transform infrared (FTIR) spectroscopy (PerkinElmer Spectrum version 10.5.1). PSCs devices performance was carried out under illumination of incandescent lamps with a power of 40 Watt at a distance of 5 cm. The PSCs object is subjected to light with a certain intensity on the top electrode (anode). The digital multimeter is connected to both electrodes with positive pole at the cathode and negative pole at the anode.

3 Results and Discussion

3.1 Structural and Physicochemical Properties of $CaTiO_3$ Powder

1.1.1 Morphologies of $CaTiO_3$ powder

Figure 1 a-d show SEM micrographs of well-defined raw material ($CaCO_3$ and TiO_2) and synthesized perovskite $CaTiO_3$ particles with the different molar ratio. It can be

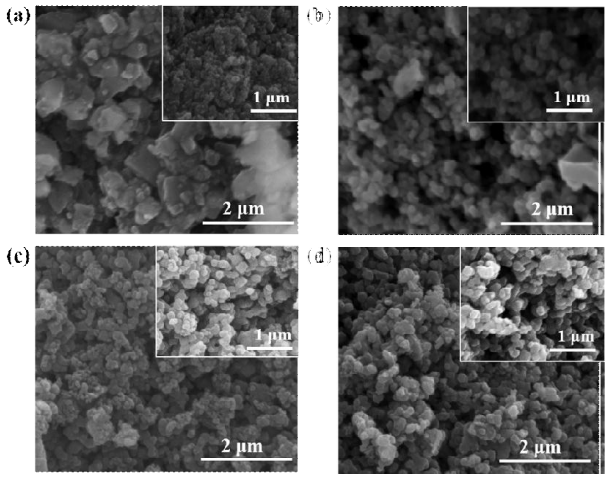

Fig. 1. SEM images of (a) $CaCO_3$ powder, (b) TiO_2 anatase powder and $CaTiO_3$ powder synthesized from $CaCO_3$:TiO_2 = (c) 1:1 and (d) 1:7 at 900°C.

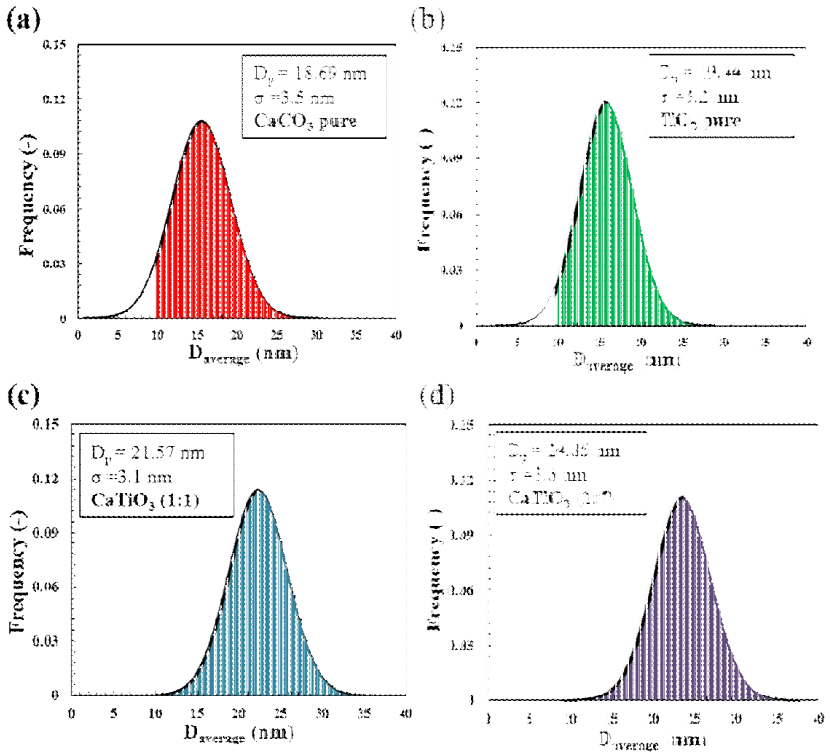

Fig. 2. Particle size distributions measured by ruler software SEM images analyses

seen that all the samples have spherical morphologies, except for $CaCO_3$ (Fig. 1a) which has a non-spherical morphology. The non-spherical shape may come from hygroscopic nature of $CaCO_3$ which is very sensitive to react with the water content from the environment humidity. This reason is in line with the Zhao et al. [20] study explaining that small variations in water content can cause the significant shape changes. As shown in Fig. 1c-d, all of the $CaTiO_3$ powders exhibit an ultra-agglomeration powder with the size of roughly 100 ± 25 nm. They are robustly agglomerated due to the highly chemically active particles [21]. It is worth noting that the synthesized $CaTiO_3$ powders are spreading more evenly and uniformly than those of $CaCO_3$ and TiO_2 powders, which gives an exceptional uniform morphology of perovskite crystal formation.

Figure 2 a-d show the particle size distribution of the raw materials and $CaTiO_3$ perovskite powders prepared by sol-gel method. As can be seen, the calculated mean diameter particle size for all of the samples are almost similar with the narrow particle size distribution about 21 ± 3 nm, suggesting that all of the samples are nanostructured particles. As shown in Fig. 2c-d, all $CaTiO_3$ powders (D_p = 21.57 and D_p = 24.85 nm) contained larger particles than those of the raw materials of $CaCO_3$ (D_p = 18.69 nm) and TiO_2 (D_p = 19.44 nm) due to the strong agglomeration process occurred (vide supra). The reactant particles ($CaCO_3$ and TiO_2) with smaller particle size were robustly agglomerating each other to form the $CaTiO_3$ perovskite products with larger particle size. These results suggesting that sol-gel method can be an effective method to fabricate narrow particle size distribution of $CaTiO_3$ perovskite material product [16].

Further observation shows that the particle size grows up as the ratio of TiO_2 increase (Fig. 2d) which is in a good agreement with XRF and XRD results (vide infra). $CaTiO_3$ powders with $CaCO_3$:TiO_2 ratio of 1:7 (Fig. 2d) have slightly larger diameter particle than the ratio of 1:1 due to the high percentage of TiO_2 composition exist in $CaTiO_3$ powders (Table 1, Fig. 1, Fig. 5). It can be noted that TiO_2 has larger diameter particles than those of $CaCO_3$ in its pure form (Fig. 2a-b), contributing to the increasing bulk particle size of $CaTiO_3$ in the agglomeration process.

1.1.2 Chemical composition of $CaTiO_3$

The chemical composition of $CaTiO_3$ powder were measured using two methods, that are XRF (Table 1, Figure 3) and FTIR (Figure 4). As shown in Table 1, the main composition in the $CaTiO_3$ is calcium and titanium which more than 16% and more than 53%, respectively. As increasing TiO_2 molar ratio from 1 to 7 respect to 1

Table 1. Chemical elements composition present in $CaTiO_3$ perovskite powder at annealing temperature of 900°C.

Elements (weight %)	Variable $CaCO_3$:TiO_2	
	1:1	**1:7**
Ca	43.11	16.22
Ti	53.37	78.46
V	1.24	1.53
Fe	1.49	2.89
Ni	0.35	0.41
Cu	0.16	0.20
Zn	0.09	0.11

molar $CaCO_3$, the composition of titanium increases fifty percent. This sharp increase due to the raw material sources of titanium in the synthesis of calcium titanate are anatase phase which has the highest percentage of TiO_2 (98%) among the other phase of TiO_2 [9].

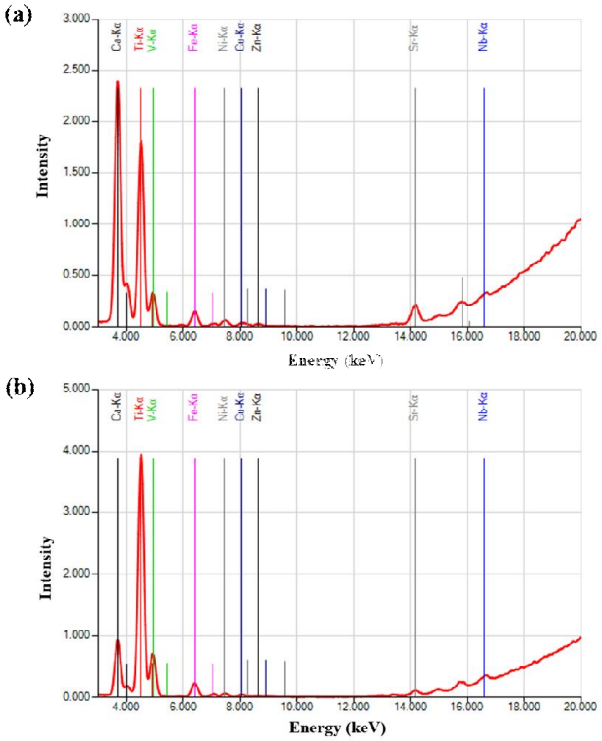

Fig. 3. XRF images of $CaTiO_3$ powder with the $CaCO_3$:TiO_2 molar ratio of (a) 1:1 and (d) 1:7 at 900°C.

The FTIR spectra of $CaTiO_3$ with different $CaCO_3$:TiO_2 molar ratio synthesized at 900°C by sol-gel method are shown in Figure 4. As shown in molar ratio of 1:1 and 1:5 FTIR graph, some peaks in the range of 3600 - 3000 cm^{-1} band are exist. It has been assigned to the O – H stretching modes of surface absorbed water corresponding to the symmetric and assymmetric stretching vibration of weakly bound water interacting with its environment via hydrogen bonding and to stretching vibrations of hydrogen-bonded OH groups [22]. As molar ratio increase to 1:7, there was no peak found indicating that absence of moisture and water molecular in this system [23]. Hence, molar ratio of 1:7 is the best condition to form a water free content of $CaTiO_3$ perovskite powders.

The band at ~1423 cm^{-1} (for molar ratio of 1:3 and 1:7) is due to a weaker, symmetrical stretching band ν(C–O) [24]. In addition, the band of $CaTiO_3$ (with molar ratio of 1:1) at 1415 cm^{-1} is assigned to carboxylic group [19]. The broad bands observed in the sample with molar ratio of 1:3 and 1:7 are at 1338 – 931 cm^{-1} are contributed to O – H bonded to titanium [25]. The interesting part in FTIR spectra (Fig. 4) is as molar ratio of TiO_2 decrease, the peak become slightly shifted into the smaller wavelength (886.75 cm^{-1}, 877.96 cm^{-1}, 875.19 cm^{-1} for molar ratio of 1:7, 1:3, 1:1, respectively). It is known first that the peaks between 1200 – 700 cm^{-1} indicate the Ti-O bonds vibration [26]. Hence, the shifting to the smaller wavenumber gives less energy required by titanium and oxygen atoms to vibrate with their certain number [27]. As a result, it can be seen that the peak of molar ratio 1:1 corresponding to the bonding of Ti-O bond length becomes increasingly elongated in the cell size.

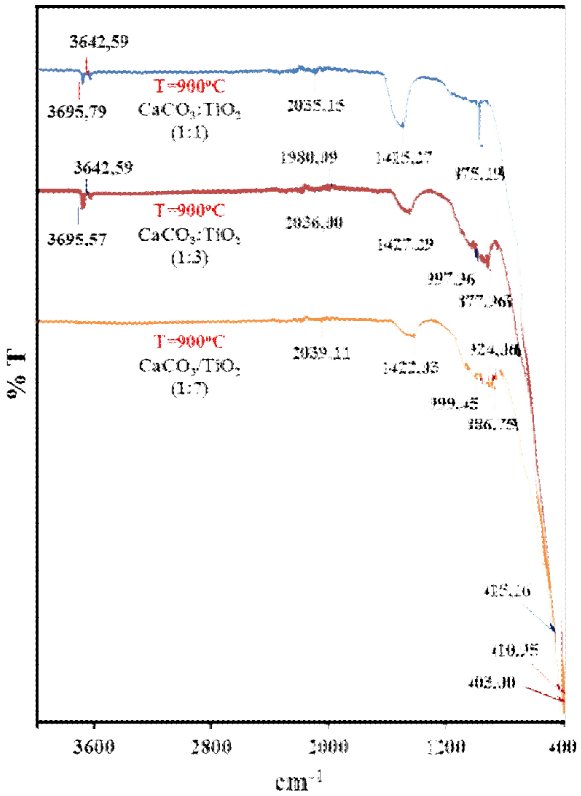

Fig. 4. FTIR spectra of $CaTiO_3$ with different raw material molar ratio prepared at 900°C.

The broad peaks of all samples are observed at the range of 700–400 cm^{-1} which is due to the Ti – O stretching vibration [19]. The most intense peaks is found in a range 573 – 420 cm^{-1}, indicating the presence of calcium titanate in all samples [28]. It clearly indicates that sol-gel method is a well-established synthetic routes to prepare calcium titanate perovskite materials.

1.1.3 XRD analysis of $CaTiO_3$

Figure 5 shows X-Ray diffraction patterns for $CaTiO_3$ powders heat treated at 600°C and 900°C with different precursor molar ratio. All the produced powders have similar XRD patterns and exhibit highly pure crystalline $CaTiO_3$ with the growth orientation along (1 2 1) direction. Their diffraction peaks match well with JCPDS card No. 22-0153 having orthorhombic structure with space group Pbnm and lattice parameter a = 5.441 Å, b = 7.643 Å and c = 5.381 Å [15,20]. It implies that the pure high crystallinity of $CaTiO_3$ powders with Pbnm orthorhombic crystal structure can be prepared from the sol-gel method with above mentioned molar ratio.

As comparison, JCPDS card No. 21-1272 and No. 37-1497 for TiO_2 anatase phase and CaO are presented to check if there any undesired phases such as TiO_2 and

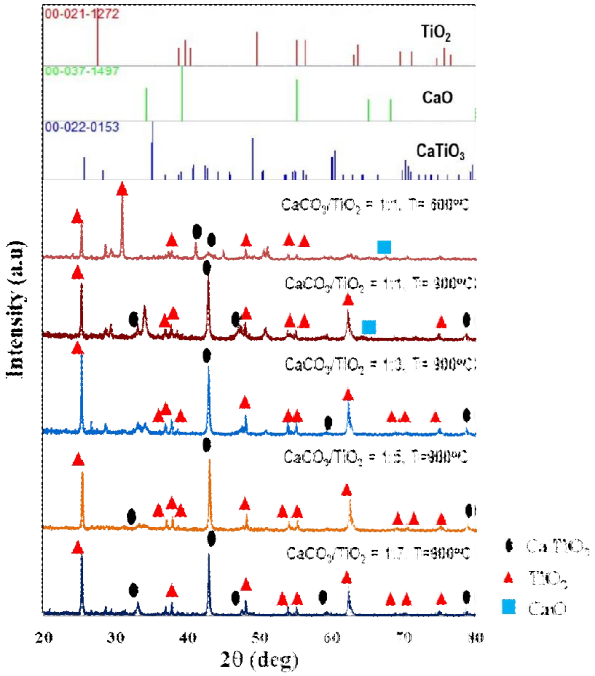

Fig. 5. XRD patterns of $CaTiO_3$ powders with different heating treatment temperature and molar ratio, as well as the JCPDS card of $CaTiO_3$, $CaCO_3$ and TiO_2 for comparison.

CaO detected in XRD pattern of prepared powders. At a $CaCO_3$:TiO_2 molar ratio of 1:1 with different heating treatment (600°C and 900°C), it is seen that there are several peaks of minor intensity corresponding to the precursor phases CaO is still observed, together with TiO_2 peaks. In addition, there were no traces of CaO in $CaTiO_3$ powders with the increasing TiO_2 molar ratio. These results are similar with Mallik et al. work, indicating that the degree of crystallization of $CaTiO_3$ powders is dependent on the mechanisms of hydrolysis and polycondensation reactions of the mixture rather than the calcination temperature of drying powders [16].

Scherrer's equation (Eq. 1) was used to measure the average crystallite size of $CaTiO_3$ powder. It can be calculated by using the full width at half maximum (FWHM) of the most intense peak at the (1 2 1) plane. According to the literature [29], the Scherrer's equation is described below:

$$D = 0.9\lambda / B \cos\theta \qquad (1)$$

where D is average crystallite size or particle size, λ is X-ray wavelength, θ is the Bragg angle and B is the FWHM.

Degree of crystallinity and crystal size of $CaTiO_3$ with the different raw material molar ratio and heating treatment are listed in Table 2. As shown, the degree of crystallinity of all $CaTiO_3$ powders are around 90%, implying that all of the synthesized CaTiO3 powders is a high crystalline nanostructure perovskite material. It can be seen that increasing heating treatment temperature (600°C to 900°C), the smaller average crystallite size is obtained. It is due to the diffusion of atoms become faster as the sintering temperature increase, thus increasing the crystallinity and forming a smaller crystal size [30]. However, the different trend line is observed with the increasing of TiO_2 ratio in the $CaTiO_3$ bulk promotes. As TiO_2 ratio increase, the mean value of crystallize size or particle size is increasing, which shows a good agreement with the measured particle size distribution from SEM analysis (Fig. 2). This behaviour can be ascribed to the aggregates production and nuclei formation [31].

Table 2. Degree of crystallinity and crystal size of $CaTiO_3$ powder with the different preparing conditions.

Variable $CaCO_3$:TiO_2	FWHM	Crystallinity (%)	Crystal size (nm)
1:1 (600°C)	0.19	88.56	25.30
1:1 (900°C)	0.18	96.68	17.70
1:3 (900°C)	0.17	97.19	22.93
1:5 (900°C)	0.15	97.43	34.07
1:7 (900°C)	0.13	97.61	40.27

3.2 Device Performance

The successfully synthesized $CaTiO_3$ perovskite powder is applied onto the active layer of perovskite solar cells device, as can be seen in Figure 6. The schematic illustration of mesoporous heterojunction n-i-p architecture of PSCs with the configuration of ITO/TiO_2/$CaTiO_3$/C/ITO are shown in Fig. 6a. According to Zhou *et al.* [32] work, mesoporous architecture was better used for providing high surface area for appropriate perovskite loading. Fig. 6b shows the photograph of lead-free PSCs devices using synthesized $CaTiO_3$ powders as an active perovskite layer.

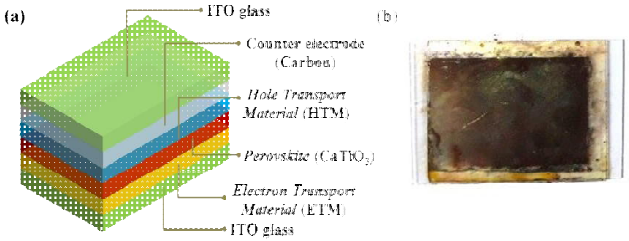

Fig. 6. (a) Schematic diagram and (b) photograph of $CaTiO_3$-based PSCs device.

The photovoltaic output parameters of PSCs with the different variable conditions are listed in Table 3. The highest efficiency is achieved by $CaTiO_3$ perovskite material with the condition of highest TiO_2 ratio (1:7) at 900°C. The more Ti content (XRF, Fig. 3) reinforced by the more Ti – O bonding (FTIR, Fig. 4) and TiO_2 intensity peaks in XRD (Fig. 5) at that condition (1:7, 900°C), suggesting that the high TiO_2 content of perovskite polycrystals can infiltrate into the pores of TiO_2 (act as electron transport material, ETM) improving the PCEs [33]. As shown in Table 3, the cells made from $CaTiO_3$ perovskite powders exhibited higher V_{OC} than those of TiO_2. The V_{OC} values depend on the difference between the Fermi level of the oxide and the redox potential of electrolyte, resulting in higher V_{OC} [34].

Table 3. Photovoltaic output parameters of PSCs with different TiO_2 molar fraction and different annealing temperature.

Variable $CaCO_3$:TiO_2	J_{SC} (mA/cm^2)	V_{OC} (V)	FF	PCE (%)
1:1 (600°C)	0.024	0.198	0.226	0.549
1:3 (600°C)	0.016	0.102	0.437	0.607
1:5 (600°C)	0.018	0.156	0.455	0.738
0:1 (900°C)	0.007	0.083	0.606	0.245
1:1 (900°C)	0.013	0.126	0.471	0.635
1:3 (900°C)	0.012	0.110	0.687	0.706
1:5 (900°C)	0.023	0.185	0.415	1.386
1:7 (900°C)	0.027	0.212	0.539	2.031

4 Conclusion

The $CaTiO_3$ perovskite material have been successfully synthesized by sol-gel method. From the investigation of structural and physichochemical properties of the synthesized $CaTiO_3$, the $CaCO_3$:TiO_2 molar ratio of 1:7 and heating temperature of 900°C give the best condition to form orthorhombic $CaTiO_3$ crystal structure and applied it onto the active area of lead-free PSCs application. The highest PCE obtained of up to 2.12% with J_{SC} value of 0.027 mA cm^{-2}, V_{OC} of 0.212 V and FF of 53.9%. This sample can be an alternative way to create lead-free, large-scale, and low-cost perovskite solar cells.

We acknowledge Central Laboratory of Malang State University for several samples characterization device. This work was supported by Lembaga Penelitian dan Pengabdian Masyarakat (LPPM) Institut Teknologi Kalimantan, Indonesia.

References

1. M. H. Hasan, T. M. I. Mahlia, H. Nur, Renew. Sustain. Energy Rev. **16**, 2316 (2012)
2. N. A. Handayani, D. Ariyanti, Int. J. Renew. Energy Dev. **1**, 33 (2012)
3. H. Zhang, J. Shi, L. Zhu, Y. Luo, D. Li, H. Wu, Q. Meng, Nano Energy **43**, 383 (2018)
4. A. Kojima, K. Teshima, Y. Shirai, T. Miyasaka, J. Am. Chem. Soc. **131**, 6050 (2009)
5. S. Yang, W. Fu, Z. Zhang, H. Chen, C.-Z. Li, J. Mater. Chem. A **5**, 11462 (2017)
6. F. Giustino, H. J. Snaith, ACS Energy Lett. **1**, 1233 (2016)
7. M. K. Assadi, S. Bakhoda, R. Saidur, H. Hanaei, Renew. Sustain. Energy Rev. **81**, 2812 (2018)
8. A. Krause, W. M. Weber, D. Pohl, B. Rellinghaus, A. Kersch, T. Mikolajick, J. Phys. D. Appl. Phys. **48**, 415304 (2015)
9. G. Gralik, C. Zanneli, F. Raupp-Pereira, M. Dondi, J. A. Labrincha, D. Hotza, In Congrs Brsl. de Eng. e Ciênc. dos Mat., 503 (2014)
10. H. Lee, T. Mizoguchi, T. Yamamoto, Y. Ikuhara, Mater. Trans. **50**, 977 (2009)
11. R. Ali, M. Yashima, J. Solid State Chem. **178**, 2867 (2005)
12. R. Rothenberg, Anatase. *https://www.mindat.org/user-3235.html*, https://www.mindat.org/min-213.html (2014)
13. T. Luttrell, S. Halpegamage, J. Tao, A. Kramer, E. Sutter, M. Batzill, Sci. Rep. **4**, 1 (2015)
14. S. Yin, D. Chen, W. Tang, Y. Peng, Mater. Sci. Eng. B Solid-State Mater. Adv. Technol. **136**, 193 (2007)
15. D. K. Singh, J. Manam, AIP Conf. Proc., 1728 (2016).
16. P. K. Mallik, G. Biswal, S. C. Patnaik, S. K. Senapati, IOP Conf. Ser. Mater. Sci. Eng., 75 (2015)
17. T. R. N. Kutty, R. Vivekanandan, Mater. Lett. 5, 79 (1987)
18. G. Gralik, A. Thomsen, C. Moraes, F. Raupp-Pereira, D. Hotza, Process. Appl. Ceram. **8**, 53 (2014)
19. M. R. Mohammadi, D. J. Fray, J. Sol-Gel Sci. Technol. **68**, 324 (2013)
20. H. Zhao, Y. Duan, X. Sun, New J. Chem. **37**, 986 (2013)
21. S. Manafi, M. Jafarian, Int. Journal of Phys. Sci. **8**, 1277 (2013)
22. A. Abdel Aal, T. R. Hammad, M. Zawrah, I. K. Battisha, A. B. Hammad, Acta Phys. Pol. A **126**, 1318 (2014)
23. S. S. Gaikwad, A. V. Borhade, V. B. Gaikwad, Der Pharma Chem. **4**, 184 (2012)
24. M. Cernea, O. Monnereau, P. Llewellyn, L. Tortet, C. Galassi, J. Eur. Ceram. Soc. **26**, 3241 (2006)
25. M. N. Kamalasanan, N. D. Kumar, S. Chandra, J. Mater. Sci. **31**, 2741 (1996)
26. C. S. Wu, J. Polym. Sci. Part A Polym. Chem. **43**, 1690 (2005)
27. F. D. Hardcastle, I. E. Wachs, Solid State Ion. **45**, 201 (1991)
28. A. I. Becerro, M. A. Carpenter, T. B. Ballaran, F. Seifert, Phase Transitions **71**, 161 (2000)
29. L. S. Cavalcante, V. S. Marques, J. C. Sczancoski, M. T. Escote, M. R. Joya, J. A. Varela, M. R. M. C. Santos, P. S. Pizani, E. Longo, Chem. Eng. J. **143**, 299 (2008)
30. P. Alpionita, Astuti, J. Fis. Unand **4**, 167 (2015)
31. G. Zhou, M. Lü, F. Gu, D. Xu, D. Yuan, J. Cryst. Growth **276**, 577 (2005)
32. L. Meng, J. You, T.-F. F. Guo, Y. Yang, Acc. Chem. Res. **49**, A (2015)
33. I. Mesquita, L. Andrade, A. Mendes, Renew. Sustain. Energy Rev. **82**, 2471 (2018)
34. Y. Okamoto, Y. Suzuki, J. Ceram. Soc. Jpn. **122**, 728 (2014)